Journal Pre-proof

Easy-plane magnetic anisotropy in layered $GdMn_2Si_2$ compound with easy-axis magnetocrystalline anisotropy

E.G. Gerasimov, P.B. Terentev, A.F. Gubkin, H.E. Fischer, D.I. Gorbunov, N.V. Mushnikov

PII: S0925-8388(19)34148-9

DOI: https://doi.org/10.1016/j.jallcom.2019.152902

Reference: JALCOM 152902

To appear in: *Journal of Alloys and Compounds*

Received Date: 29 August 2019

Revised Date: 25 October 2019

Accepted Date: 1 November 2019

Please cite this article as: E.G. Gerasimov, P.B. Terentev, A.F. Gubkin, H.E. Fischer, D.I. Gorbunov, N.V. Mushnikov, Easy-plane magnetic anisotropy in layered $GdMn_2Si_2$ compound with easy-axis magnetocrystalline anisotropy, *Journal of Alloys and Compounds* (2019), doi: https://doi.org/10.1016/j.jallcom.2019.152902.

Easy-plane magnetic anisotropy in layered $GdMn_2Si_2$ compound with easy-axis magnetocrystalline anisotropy

E. G. Gerasimov[1,2], P. B. Terentev[1,2], A. F. Gubkin[1,2], H. E. Fischer[3], D. I. Gorbunov[4], N. V. Mushnikov[1,2]

[1]*M.N. Miheev Institute of Metal Physics of Ural Branch of Russian Academy of Sciences, Kovalevskaya str. 18, 620108 Ekaterinburg, Russia*

[2]*Institute of Natural Sciences and Mathematics, Ural Federal University, Mira str. 19, Ekaterinburg, Russia*

[3]*Institut Laue-Langevin, 71 avenue des Martyrs, CS 20156, 38042 Grenoble cedex 9, France*

[4]*Hochfeld-Magnetlabor Dresden (HLD-EMFL), Helmholtz-Zentrum Dresden-Rossendorf, 01328 Dresden, Germany*

**Corresponding author e-mail: gerasimov@imp.uran.ru*

Abstract

Magnetic properties and magnetic structures of layered $GdMn_2Si_2$ compound were studied using quasi-single crystal, high magnetic fields up to 520 kOe, and neutron powder diffraction experiment designed for high absorbent systems. It was shown that $GdMn_2Si_2$ has strong easy plane type magnetic anisotropy at temperatures $T_{Gd} < 52$ K at which Gd atoms are magnetically ordered. At temperatures 52 K < T < 453 K, the compound has antiferromagnetic ordering of Mn layers and easy axis type magnetic anisotropy with the easy axis directed along the tetragonal *c*-axis. The exchange-induced in-plane magnetic anisotropy of layered $GdMn_2Si_2$ at low temperatures arises to prevent magnetic frustration in Gd layers. Magnetic properties of $GdMn_2Si_2$ at temperatures below 52 K can be described within a three-sublattice model based on the Yafet-Kittel approximation.

Keywords: magnetic anisotropy; magnetic frustration; magnetic phase transitions; magnetic structures

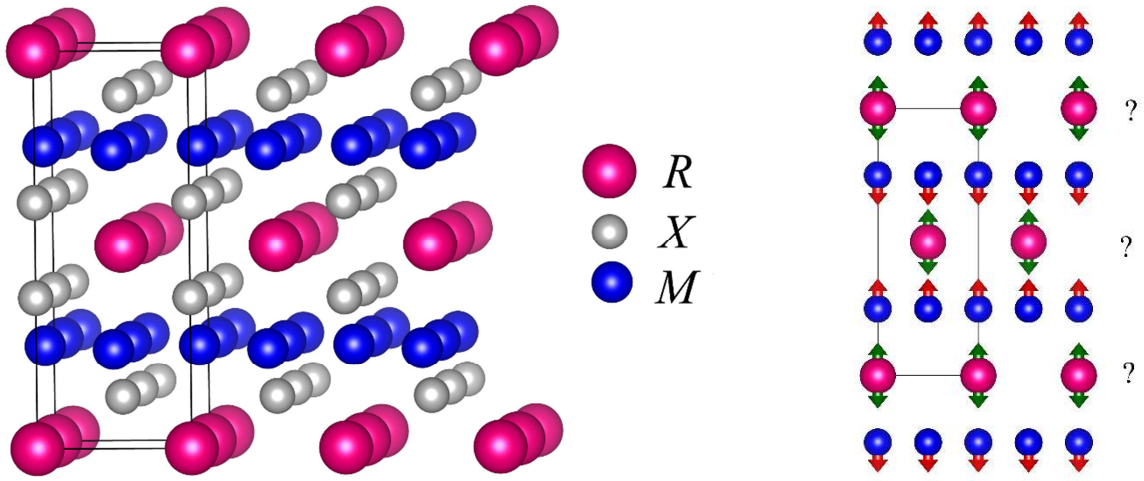

Fig.1. Illustration of layered crystal structure of the RM_2X_2 compounds (left side) and origin of magnetic frustration in RMn_2X_2 compounds with $d_{Mn\text{-}Mn} < d_{crit1}$ (right side).

Introduction

Intermetallic RM_2X_2 compounds (R is the rare earth metal, M is 3d, 4d or 5d transition metal and X = Si or Ge) crystallize in the tetragonal $ThCr_2Si_2$-type structure which represents ideal natural multilayered system. The structure consists of the R, M and X monoatomic layers stacked along the crystallographic c axis in strong -M-X-R-X-M- sequence (Fig. 1a). The coexistence of layers with elements from various groups of the Periodic table stipulates unusually wide range of physical phenomena for the compounds. These phenomena include superconductivity, heavy fermions, crystal electric fields effects, mixed valence, manifold magnetic structures and magnetic phase transitions [1, 2]. Correspondingly, the RM_2X_2 compounds

are attractive objects for both various theoretical model studies and magnetoelastic and magnetocaloric applications, for which the magnetic phase transitions play crucial role.

Rich variety of magnetic phase transitions and magnetic structures in the RM_2X_2 compounds with M = Mn mainly arises from a competition between interlayer R-R, R-Mn, and Mn-Mn exchange interactions. The R-Mn exchange interactions obey common rule for R-M compounds (were R- is rare-earth element, M -3d transition metal) and are ferromagnetic for “light” and antiferromagnetic for “heavy” rare-earth elements. The Mn-Mn interlayer exchange interaction unusually strongly depends on intralayer Mn-Mn distance $d_{Mn\text{-}Mn}$. Two critical intralayer Mn-Mn distances are typically observed in the compounds: $d_{crit1} \approx 0.287$ nm and $d_{crit2} \approx 0.284$ nm. At $d_{Mn\text{-}Mn} > d_{crit1}$, the interlayer Mn-Mn exchange coupling is ferromagnetic and the intralayer Mn-Mn coupling is antiferromagnetic. At $d_{crit2} < d_{Mn\text{-}Mn} < d_{crit1}$, both the interlayer and

intralayer Mn-Mn couplings are antiferromagnetic. At $d_{\text{Mn-Mn}} < d_{\text{crit2}}$, there is no intralayer in-plane spin component and interlayer Mn-Mn coupling is antiferromagnetic. Correspondingly, the magnetic ordering in many cases can be tuned by change of intralayer Mn-Mn distance by variation of the concentration of *R* elements in quasi-ternary $R_{1-x}R`_{x}Mn_2(Si_{1-y}Ge_y)_2$ compounds [3, 4, 5, 6, 7, 8].

Another important mechanism that affects the formation of magnetic structures in RM_2X_2 is a competition between magnetic anisotropies of the *R* and Mn subsystems. This mechanism has not been studied properly up to now. The Mn layers usually demonstrate strong uniaxial anisotropy with the easy axis directed along the tetragonal *c*-axis of the RMn_2X_2 structure [9, 10, 11]. The *R* sublattice anisotropy can be both the easy axis and easy plane type. Various combinations of magnetic anisotropies and interlayer *R-M* and *M-M* exchange interactions result in formation of unusual magnetic states in layered RMn_2X_2 compounds. The most interesting situations are realized when $d_{\text{Mn-Mn}} < d_{\text{crit1}}$ because magnetic moments of each of *R* layer should be either parallel or antiparallel to two adjacent antiferromagnetically coupled Mn layers, which leads to magnetic frustrations (Fig.1b). In this case, the anisotropies competition may lead to violation of above-mentioned relationship between type of interlayer Mn-Mn magnetic ordering and intralayer Mn-Mn distance. For example, ferromagnetic interlayer Mn-Mn ordering was found in $TbMn_2Si_2$ and $DyMn_2Si_2$ at low temperatures at which the *R* sublattice is magnetically ordered, in spite of $d_{\text{Mn-Mn}} < d_{\text{crit1}}$ [12, 13]. Recently it was also shown that, due to the frustrations in Tb magnetic subsystem, the Mn-Tb and Tb-Tb interlayer exchange competition and strong easy-axis magnetocrystalline anisotropy of both the Tb and Mn sublattices prevents long-range magnetic ordering in the rare-earth sublattice of $La_{1-x}Tb_xMn_2Si_2$ [14]. The existence of the frustrated state was proposed using magnetic measurements on single crystal samples and then was confirmed by magnetic neutron powder diffraction studies [15].

Recently, using bulk magnetization data, we found that $La_{1-x}Gd_xMn_2Si_2$ compounds with $x > 0.2$ exhibit strong in-plane magnetic anisotropy, though the Mn layers have easy-axis type magnetic anisotropy [16]. These findings allow tailoring the type and value of magnetic anisotropy by adjusting exchange interactions in the intermetallic compounds, which is important for practical applications. The aim of this work is to provide direct evidences of formation of such unusual magnetic structures and explore the effect of external magnetic field on magnetic phase transitions in such systems. Here we report the results of our studies of $GdMn_2Si_2$ with $d_{\text{Mn-Mn}} < d_{\text{crit1}}$ using high magnetic fields measurements on quasi-single crystal sample and neutron powder diffraction with D4 (ILL, France) diffractometer that was specially designed for high absorbent systems containing Gd.

Experimental details

The $GdMn_2Si_2$ alloy was prepared by induction melting of the constituents in an argon atmosphere followed by annealing at 900°C for one week. According to the powder X-ray diffraction analysis, the alloy is single-phase with the tetragonal $ThCr_2Si_2$-type structure, the lattice parameters at room temperature being a = 0.39546 nm, c = 1.05191 nm. The intralayer Mn-Mn distance $d_{Mn\text{-}Mn} = a/\sqrt{2}$ = 0.2796 nm is considerably lower than $d_{crit1} \approx 0.287$ nm and $d_{crit2} \approx 0.284$ nm. No detectable traces of impurity phases even as minor reflections were discernible. For the magnetization studies, the quasi-single-crystal sample in the form of plate with the mass of 12 mg was selected from large grains of the ingot. The demagnetization factor of the sample N was estimated for the case of a circular cylinder with radius r, length $2nr$ and dimension ratio n = 2 using relation from Ref. [17]. We used the estimated values of the demagnetization factor when processing magnetization curves. X-ray back-scattered Laue analysis confirmed that the plate consists of several crystallites, the tetragonal c-axes of which are oriented strictly perpendicular to the plate plane, while the a-axes of crystallites are partially disoriented within the plane of the plate. In order to avoid rotation in magnetic field, the quasi-single crystal in a cube of the epoxy resin was glued in a way that the c-axis of the samples was oriented parallel to the cube edge.

The magnetization measurements of quasi-single-crystal sample in magnetic fields up to 50 kOe were performed in the Center of Collective Use of IMP UB RAS with Quantum Design MPMS5-XL SQUID magnetometer at different temperatures. High-field magnetization was measured in pulsed magnetic fields up to 520 kOe (pulse duration 25 ms) by the induction method using a coaxial pickup coil system (Hochfeld-Magnetlabor Dresden, Germany). The absolute values of the magnetization were calibrated using steady-field data in magnetic fields up to 140 kOe. A detailed description of the high-field magnetometer is given in Ref. [18].

Neutron powder diffraction studies were carried out with D4 diffractometer (Institute Laue Langevin, France) with short neutron wavelength λ = 0.4959 Å, which is powerful instrument for studies of magnetic structures of very absorbent systems such as those containing Gd, Eu, Sm. The raw neutron diffraction data were corrected for angular-dependent attenuation coefficients as well as for multiple scattering by means of CORRECT program. The corrected neutron diffraction data were analyzed by the Rietveld refinement using FullProf software [19].

Experimental results and discussion

1. Magnetic properties

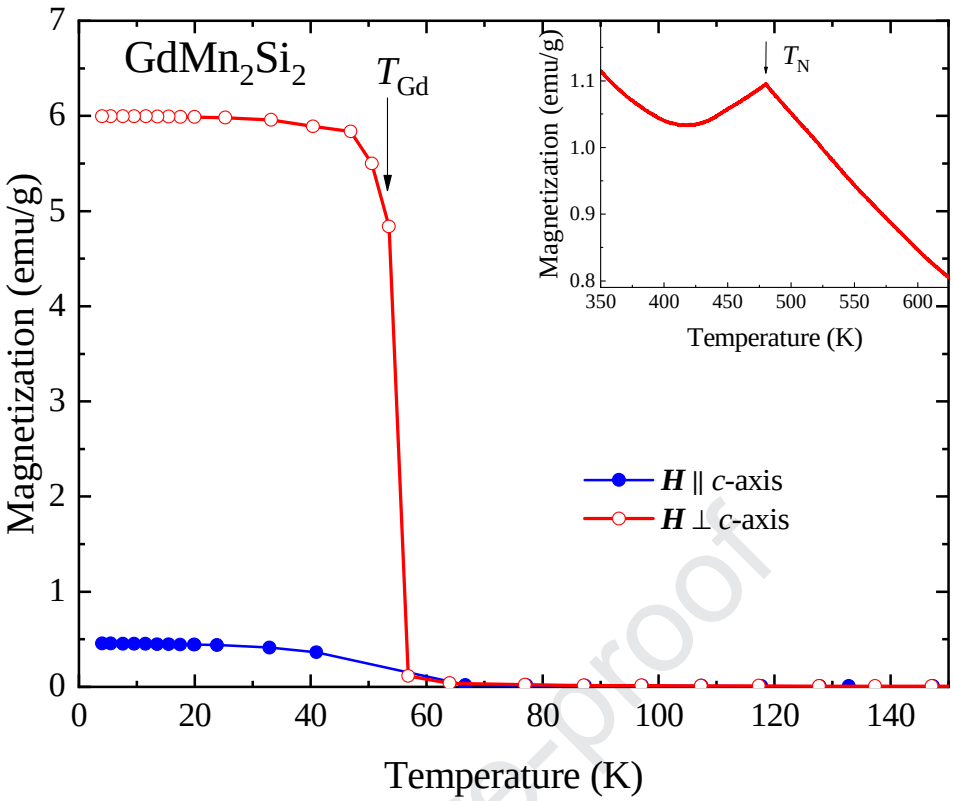

Fig. 2. Temperature dependence of the magnetization $M(T)$ of the single-crystalline sample $GdMn_2Si_2$ measured in external magnetic field H = 50 Oe applied along the c-axis and in the basal plane. Inset shows temperature dependence of magnetization near the Neel temperature T_N for polycrystalline sample in magnetic field H = 10 kOe.

Figure 2 shows the temperature dependence of the magnetization $M(T)$ of single-crystalline sample $GdMn_2Si_2$ measured in a small magnetic field of H = 50 Oe applied along the c-axis and in the basal plane. A sharp increase of the magnetization was observed for the sample cooled below T_{Gd} = 52 K. This change of magnetization can be attributed to the appearance of the long-range magnetic ordering in the Gd sublattice at $T < T_{Gd}$. The spontaneous magnetization in the basal plane was found to be much larger than the one observed along the c-axis at temperatures below T_{Gd}. It means that the easy magnetization direction of $GdMn_2Si_2$ lies in the basal plane. At temperatures $T_{Gd} < T < T_N$ = 453 K, $GdMn_2Si_2$ exhibits antiferromagnetic behavior. Maximum on $M(T)$ dependence corresponds to the Néel temperature T_N (see inset in Fig.2). At $T > T_N$, magnetic state of $GdMn_2Si_2$ is paramagnetic. Temperature dependence of the paramagnetic susceptibility obeys the Curie-Weiss law with the paramagnetic Curie temperature θ_p = 94 K and effective magnetic moment μ_{eff} = 10.5 μ_B/f.u. [16].

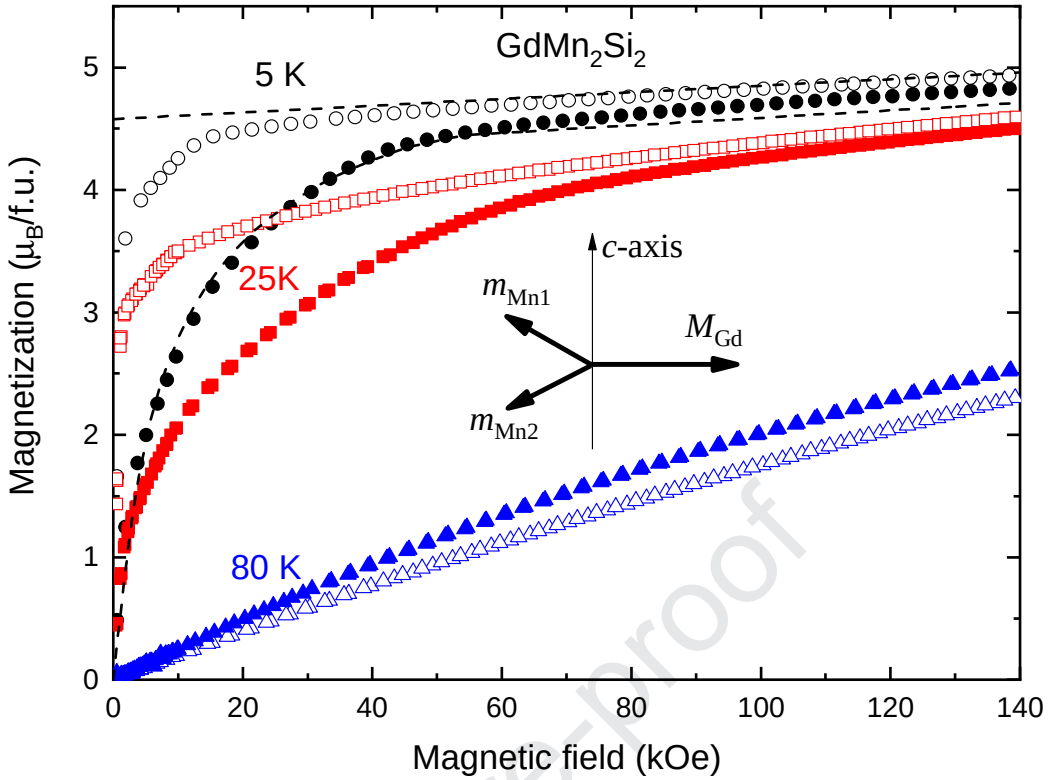

Fig.3. Magnetization curves for $GdMn_2Si_2$ along the *c*-axis (closed symbols) and in the basal plane (open symbols) at various temperatures. Scheme of triangular magnetic structure at low temperatures is also shown.

Fig. 3 shows magnetization curves of the $GdMn_2Si_2$ single crystal measured at various temperatures along the *c*-axis and in the basal plane. The data were collected during the field-down sweep. Magnetization curves at temperatures $T < T_{Gd}$ clearly indicate strong in-plane magnetic anisotropy, since application of external magnetic field along the crystallographic *c* axis results in substantially slower magnetization growth than in the geometry when magnetic field is applied in the basal plane. The shape of magnetization curves is typical for an anisotropic ferrimagnet. There observed the remanence along the easy magnetization direction. The magnetization does not reach saturation in magnetic fields up to 140 kOe even for lowest temperature. By direct summing of Gd magnetic moment μ_{Gd} = 7 μ_B and magnetic moment of two Mn atoms μ_{Mn}, the typical value in RMn_2X_2-type compounds being within range of 2 - 3 μ_B according to numerous neutron scattering studies [3, 4, 7, 8, 13, 15], the maximum magnetization values in the saturated ferromagnetic state of $GdMn_2Si_2$ can be estimated as 11-13 μ_B per formula unit.

At temperatures $T_{Gd} < T < T_N$, the Gd layers should be magnetically disordered and antiferromagnetic Mn-Mn interlayer collinear ordering is expected because $d_{Mn\text{-}Mn} < d_{crit2} < d_{crit1}$.

The studies of Mn magnetic anisotropy in $LaMn_2Si_2$ and $La_{1-x}Sm_xMn_2Si_2$ showed that Mn sublattice has strong uniaxial anisotropy with the easy axis directed along the tetragonal *c*-axis independently of type of Mn-Mn magnetic ordering [9, 11]. Correspondingly, we can expect antiferromagnetic Mn-Mn ordering along the *c*-axis and linear dependence of magnetization versus magnetic field applied along the basal plane while spin-flip or spin flop transition can be observed if the field applied along the *c*-axis [20]. However, the shape of magnetization curves looks different from the typical curves expected for a uniaxial anisotropic antiferromagnet. The magnetization at 80 K gradually and slightly non-linearly increases for both directions (Fig.3). The magnetization along the *c*-axis is slightly higher than that in the basal plane, though the difference is small. One can suggest that paramagnetism of Gd layers or non-collinear Mn-Mn magnetic ordering may give rise to non-linear behavior of magnetization of the $GdMn_2Si_2$ compound at temperatures $T > T_{Gd}$.

Summarizing the results of the above magnetic measurements, we can conclude that in-plane magnetic anisotropy arises in $GdMn_2Si_2$ at $T < T_{Gd}$. This is quite unexpected finding because Gd has no orbital momentum and magnetocrystalline anisotropy of Gd layers cannot provide significant contribution to the total anisotropy of the compound. The Mn sublattice has uniaxial anisotropy with the easy *c* axis. Magnetic measurements on the single crystal sample allow us to suggest that at $T < T_{Gd}$ there realized a triangular magnetic structure for which the Gd magnetic moments lie in the basal plane (Fig.3). Triangular magnetic structure prevents magnetic frustration in Gd layers.

Theoretically, the existence of such type magnetic structure was assumed for RMn_2X_2 within three-sublattice model [21, 22] based on the Yafet-Kittel approximation [23]. We analyzed magnetization process of $GdMn_2Si_2$ crystal using similar model. The expression for the free energy of the $GdMn_2Si_2$ in the magnetic field applied along the *c*-axis is written in the form:

$$E = -J_{GdMn}\boldsymbol{M}(\boldsymbol{m_{Mn1}}+\boldsymbol{m_{Mn2}}) - J_{MnMn}\boldsymbol{m_{Mn1}}\boldsymbol{m_{Mn2}} - K_1((m_{Mn1z})^2 + (m_{2Mnz})^2)/(2m^2) + K_2((m_{1Mnz})^4 + (m_{Mn2z})^4)/(2m^4) - \boldsymbol{H}(\boldsymbol{M} + \boldsymbol{m_{Mn1}} + \boldsymbol{m_{Mn2}}), \quad (1)$$

where $\boldsymbol{M}$ is magnetization vector of Gd sublattice; $\boldsymbol{m_{Mn1}}$, $\boldsymbol{m_{Mn2}}$ are magnetization vectors of Mn sublattices ($|\boldsymbol{m_{Mn1}}| = |\boldsymbol{m_{Mn2}}| = m$); m_{Mn1z}, m_{Mn2z} are the projections of $\boldsymbol{m_{Mn1}}$, $\boldsymbol{m_{Mn2}}$ to the tetragonal *c*-axis; J_{GdMn} is interlayer Gd-Mn exchange interaction; J_{MnMn} is Mn-Mn interlayer exchange interaction; K_1, K_2 are the anisotropy constants of the manganese sublattice. First two terms in expression (1) describe interlayer Mn-Mn and Gd-Mn exchange interactions, second two terms describe magnetic anisotropy of Mn sublattices and last term describes the Zeeman's energy. In contrast to Refs. [21, 22], we are forced to introduce the anisotropy constant K_2 in the

expression (1) for the free energy in order to describe the nonlinear nature of the magnetization. Minimization

of the expression (1) at various values of H allowed us to obtain the calculated magnetization curves for the orientation of the magnetic field parallel and perpendicular to the c-axis of the crystal. For fitting procedure, we used the data obtained in steady magnetic fields up to 140 kOe since they are measured more precisely than those in pulsed magnetic fields up to 520 kOe. Best fit of the experimental magnetization curves was obtained for the values of J_{GdMn} = -1.15 kOe/G, J_{MnMn} = -3.13 kOe/G, K_1 = 25.8×10^6 erg/cm^3 and K_2 = -5.87× 10^6 erg/cm^3. Dashed lines in Fig 3 represent the calculated magnetization curves at 4.2 K both in the basal plane and along the c-axis. The spontaneous magnetic moment of the three-sublattice magnetic structure is oriented in the basal plane parallel to the magnetic moment of gadolinium sublattice μ_{Gd}. It has a smaller value than μ_{Gd} because of an antiparallel orientation of the total moment of two Mn sublattices. Negative Gd-Mn exchange interaction forces deviation of the magnetic moments of the manganese layers with respect to the c-axis.

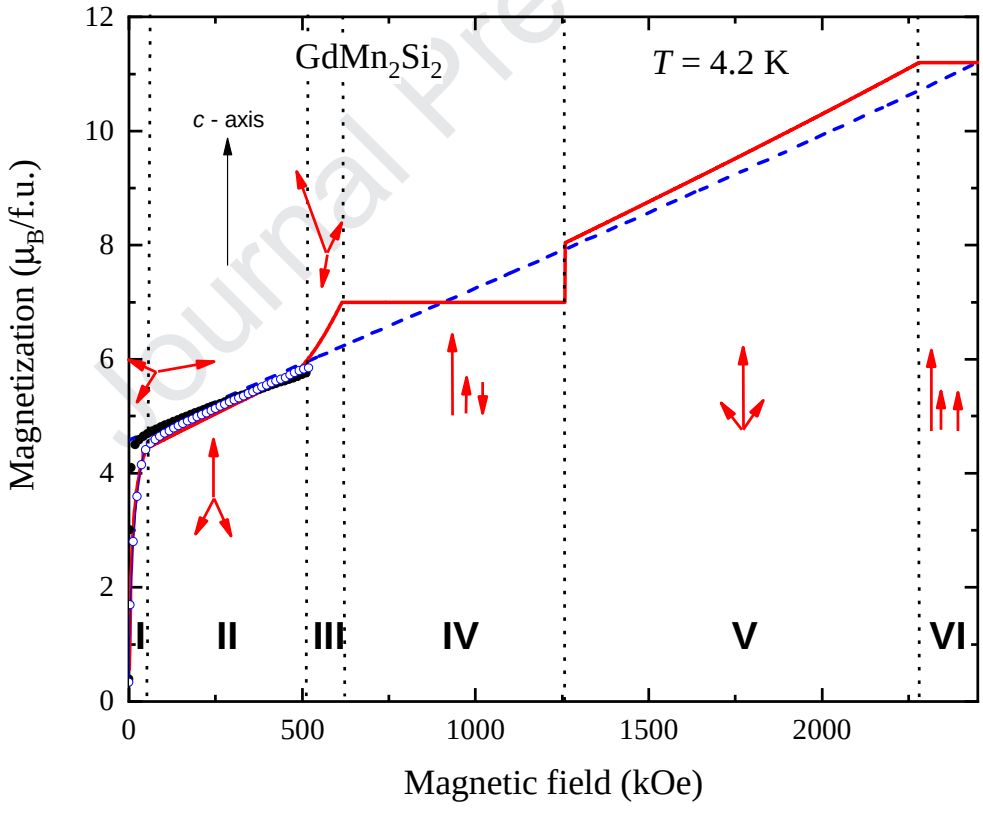

Fig.4. Experimental (symbols) and calculated (lines) magnetization curves for $GdMn_2Si_2$ along the c-axis (open symbols, solid line) and in the basal plane (closed symbols, dashed line) at T = 4.2 K. Arrows show calculated orientation of Mn (short) and Gd (long) magnetic moments in magnetic fields applied along the c-axis.

Using the obtained values of exchange parameters and anisotropy constants we are able to determine the total low-temperature magnetization processes in $GdMn_2Si_2$ up to ferromagnetic saturation. Calculated magnetization curves along *c*-axis and in basal plane are shown in Fig. 4. It is seen that application of magnetic field in the basal plane leads to a uniform rotation of the magnetic moments of manganese, and the magnetization process is linear up to saturation (dashed line). When magnetic field is applied along the *c*-axis, one can separate six stages of magnetization, which are shown by solid line in Fig. 4. At first stage (I), a rotation of triangular magnetic structure occurs, the total magnetic moment being finally oriented along the *c*-axis. At second stage (II), there occurs a small rotation of the Mn sublattices toward the field direction. For third stage (III), symmetry is broken for triangular magnetic structure and the Gd moment deviates from the *c*-axis. At fourth stage (IV), a collinear ferrimagnetic field-induced magnetic structure with zero susceptibility is formed, which remains stable up to a spin-flop transition between (IV) and (V) stages. Finally, ferromagnetic saturation is achieved (stage VI) in magnetic fields above 2300 kOe. We performed magnetic measurements in high pulsed magnetic fields to compare experimental and calculated magnetization. We found a good agreement between calculated and experimental data in experimentally reached pulsed magnetic fields up to 520 kOe (Fig.4). However, we did not rich even the third stage of magnetization.

2. Neutron diffraction

We measured neutron diffraction patterns [24] of GdMn2Si2 using the D4 instrument [25] of the Institut Laue-Langevin (Grenoble, FR) using a neutron wavelength of 0.4959 A (in order to minimize absorption effects from the Gd atoms and for various temperatures between 10 K and 300 K. All neutron diffraction patterns are collected in the 2D plot in Fig. 5. The highest temperature in our neutron diffraction experiment is still much below the Neel temperature of Mn sublattice T_N = 453 K. No appreciable changes in the neutron diffraction patterns is observed in the temperature range $T_{Gd} < T <$ 300 K. However, cooling the sample below T_{Gd}=52 K results in substantial increase of magnetic contribution to (101) and (002) Bragg peaks as well as decrease of the background intensity in the low angles (see right panel in Fig. 5). Bearing in mind our magnetic measurements data and neutron diffraction data for isostructural $GdMn_2Ge_2$ [26], we shall call magnetic state of magnetically ordered Mn sublattice in the temperature range $T_{Gd} < T < T_N$ as a high-temperature magnetic phase. Contrary, the magnetic state involving both magnetically ordered Mn and Gd sublattices below T_{Gd} = 52 K will be denoted as a low-temperature magnetic phase.

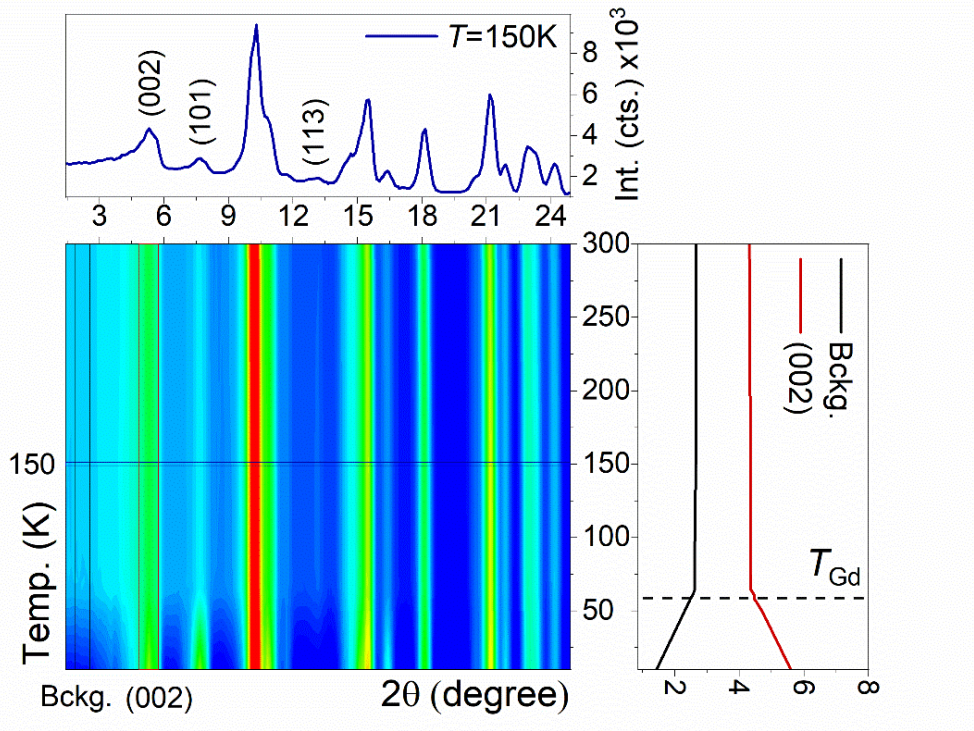

Fig. 5 Neutron diffraction patterns for $GdMn_2Si_2$ plotted as a function of temperature represented using colored 2D map. A horizontal cut at T = 150 K is shown on the top panel. Two vertical cuts representing temperature dependence of the (002) Bragg peak and background at the low angles are shown in the right panel.

Possible magnetic structures determined for the Mn sublattice in the RMn_2X_2 (X=Ge, Si) compounds have been classified by Venturini et al. [27] based on neutron diffraction data. There are five types of antiferromagnetic structures potentially adopted by Mn sublattice: AF*il*; AF*mc*; AF*mi*, AF*l* and AF*fs*. Incommensurate magnetic structures of AF*mi* and AF*fs* type can be excluded from our consideration since there are no incommensurate magnetic satellites at the neutron diffraction patterns of $GdMn_2Si_2$. The rest three AFM structures can be identified from neutron diffraction data using a number of unique characteristic Bragg peaks, as it was explained in Refs. [27, 28, 29].

(1) Antiferromagnetic ordering of Mn atoms within the (001) planes adopted by AF*l* structure gives rise to the Bragg peaks of $h + k = 2n + 1$ type (e.g. (101), (103) reflections).

(2) Collinear magnetic structure of AF*il* type exhibiting adjacent ferromagnetic Mn planes antiferromagnetically coupled along the *c*-axis gives rise to the Bragg peaks of $h + k + l = 2n + 1$ type (e.g. (111), (113) reflections).

(3) Noncollinear antiferromagnetic structure of AF*mc* type which can be represented as a superposition of AF*l* and AF*il* magnetic structures results in both h + k = 2n + 1 and h + k + l = 2n + 1 type Bragg peaks (e.g. (101), (103) and (111), (113) reflections).

As seen from Fig. 6, the neutron diffraction pattern measured at T = 300 K, exhibits both (101) and (113) Bragg peaks which implies AF*mc* type magnetic structure. The result of the Rietveld refinement using AF*mc* model is shown in Fig. 6. The refined magnetic moments and agreement factors are listen in Table 1.

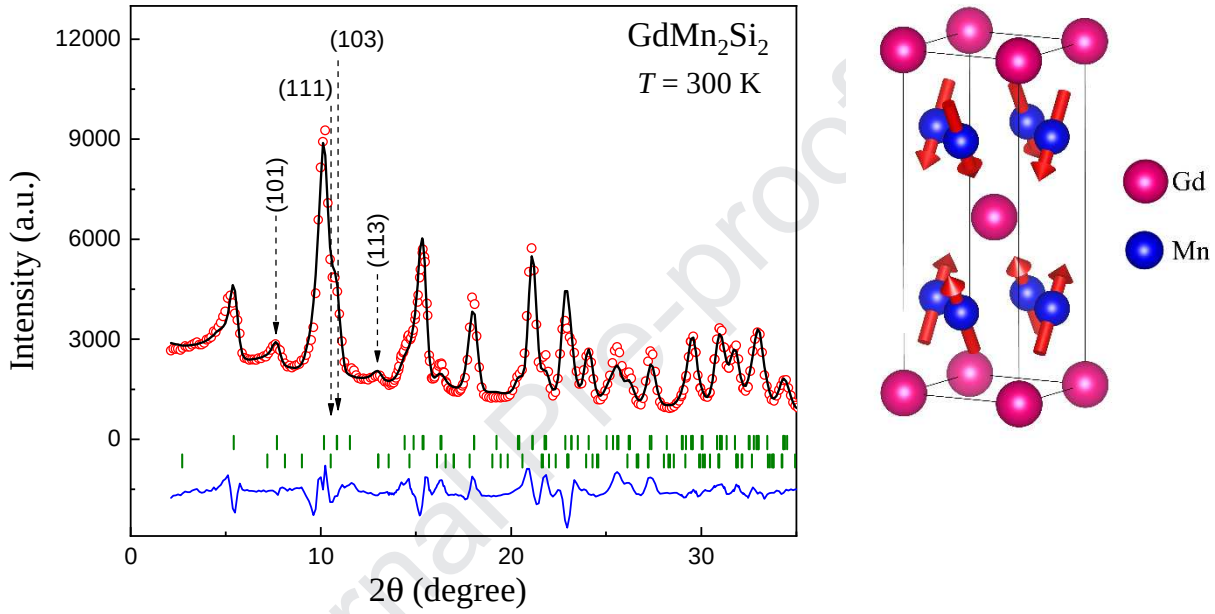

Fig.6 Neutron diffraction patterns of $GdMn_2Si_2$ at 300 K. Points are experimental data, bold lines are Rietveld refinement with FullProf. Below the patterns, vertical lines point to the positions of magnetic and nuclear reflections, thin solid line at the bottom shows the difference between the experimental and calculated patterns. At the right side, refined AF*mc* magnetic structure is shown.

Now let us consider in more details a low-temperature magnetic phase at temperatures below T_{Gd} = 52 K that corresponds to the ordering temperature of Gd magnetic moments. Previously, the authors of [23] performed neutron diffraction studies of the isostructural $GdMn_2Ge_2$ compound. However, due to larger atomic radius of Ge, the condition $d_{Mn\text{-}Mn} > d_{crit1}$ holds for $GdMn_2Ge_2$ down to lowest temperatures. Therefore, the interlayer Mn-Mn coupling is ferromagnetic. Accordingly, neutron diffraction data show simple collinear ferrimagnetic (at $T < T_{Gd}$) and antiferromagnetic (at $T_{Gd} < T < T_N$) structures [26]. For the $GdMn_2Si_2$, for which $d_{Mn\text{-}Mn} < d_{crit1}$, magnetic structures are more complex, since, as explained above, there appear conditions for magnetic frustrations. For our neutron diffraction patterns, a substantial increase of magnetic

contribution to the (002) and (101) Bragg peaks implies emergence of ferromagnetic in-plane component of Gd magnetic moments (Fig.7). These findings are in good agreement with our bulk magnetization data. According to magnetic measurements, spontaneous in-plane magnetic moment of $GdMn_2Si_2$ is about 4.6 μ_B (Fig.3) that is lower than magnetic moment of Gd^{3+} ion (μ_{Gd} = 7 μ_B). A superposition of the in-plane ferrimagnetic structure and AF*il*-type out-of-plane component of Mn sublattice observed at high temperatures gives us best Rietveld refinement of the neutron diffraction pattern measured at T = 10 K. The results of the Rietveld refinement using this model are shown in Fig. 7. The refined magnetic moments and agreement factors are listen in Table 1.

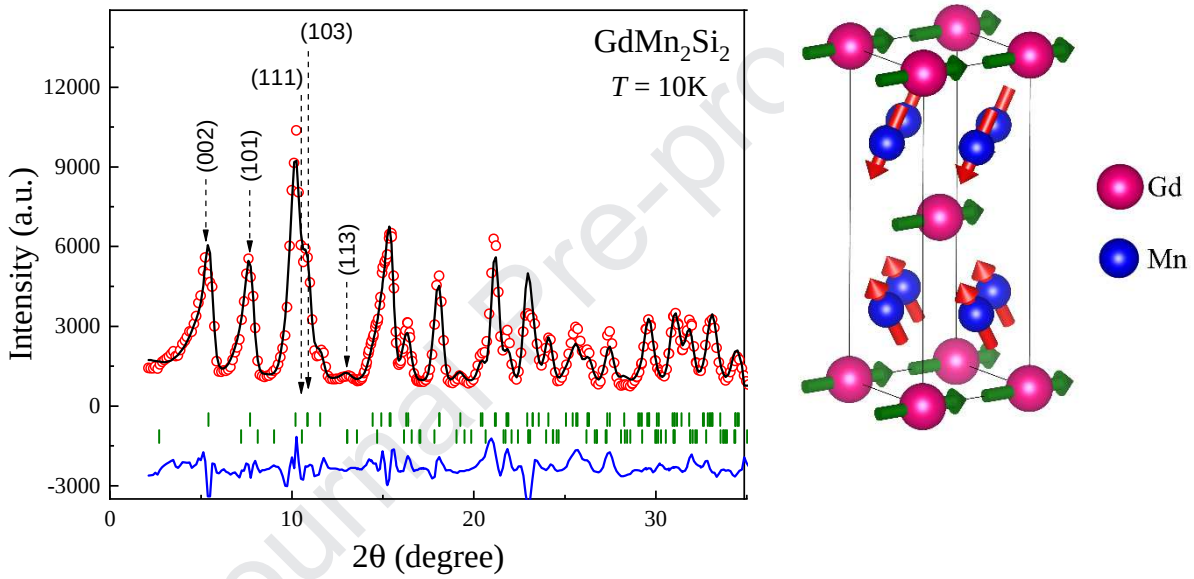

Fig.7 Neutron diffraction patterns of $GdMn_2Si_2$ at 10 K (left side). Points are experimental data, bold lines are Rietveld refinement with FullProf. Below the patterns, vertical lines point to the positions of magnetic and nuclear reflections, thin solid line at the bottom shows the difference between experimental and calculated profiles. Schematic visualization of the noncollinear magnetic structure refined at T = 10 K (right side).

Table 1. Results of Rietveld refinement of $GdMn_2Si_2$ magnetic structures at temperatures T =

10 K and 300 K. Projections of magnetic moments on *c*-axis (μ_z), basal plane (μ_x) and total magnetic moment ($|\mu|$) are given.

	μ_z	μ_x	$\|\mu\|$
T = 10 K, superposition of AF*il* out-of-plane component and ferrimagnetic in-plane component (Fig. 7)			
Mn	1.9 ± 0.2 μ_B	-1.0 ± 0.1 μ_B	2.2 ± 0.2 μ_B
Gd	0	6.7 ± 0.2 μ_B	6.7 ± 0.2 μ_B
R_{Bragg} = 9.4, R_{magn} = 17.7, χ^2 = 342			
T = 300 K, AF*mc* magnetic structure (Fig.6)			
Mn	2.0 ± 0.1	-1.4± 0.1	2.4 ± 0.2
R_{Bragg} = 6.2, R_{magn} = 14.8, χ^2 = 206			

According to the refined structure and atomic moments, the spontaneous magnetic moment in the basal plane at 10 K amounts to $\mu_{Gd} + 2\mu_x(Mn) = 4.7\ \mu_B$. This value is in good agreement with 4.6 μ_B determined from bulk magnetization measurement of the single crystal (Fig. 3). Thus, our neutron diffraction studies confirm formation of the easy-plane magnetic anisotropy for $GdMn_2Si_2$ at low temperatures.

Conclusion

We have studied magnetic properties and magnetic structures of $GdMn_2Si_2$ using high-field magnetization measurements for the quasi-single crystal sample and powder neutron diffraction with D4 (ILL, France) diffractometer that specially designed for high absorbent systems containing Gd. Our results give direct evidence of formation of non-collinear magnetic structure with in-plane magnetic anisotropy at temperature below the ordering temperature of the Gd sublattice T_{Gd} = 52 K. Above T_{Gd}, the uniaxial magnetic anisotropy of the antiferromagnetically ordered Mn sublattice is observed.

It is well known that in the *R*-*M* intermetallic compounds, due to a competition of magnetic anisotropies of the *R* and *M* sublattices, the spin-reorientation transition can be realized upon changing temperature or composition [30, 31]. Exchange interaction considerably affects temperature dependence of magnetic anisotropy constants [32]. Therefore, influence of exchange interactions to the type and value of total magnetic anisotropy of two-sublattice ferrimagnets is often observed. However, completely different situation is realized in $GdMn_2Si_2$. The sum of the second-order and firth-order anisotropy constant for $GdMn_2Si_2$ amounts to $K_1 + K_2$ = -8.4 erg/cm^3. Very similar absolute value of 7.7 erg/cm^3 was found for the isostructural $LaMn_2Si_2$

ferromagnet with non-magnetic La [9,16]. Therefore, because of zero orbital momentum of Gd, the magnetocrystalline anisotropy of the Gd sublattice is small in comparison with that of the Mn sublattice. Nevertheless, ordering of the Gd sublattice is accompanied by reorientation of the easy magnetization direction.

We consider that the unusual magnetic ordering is due to appearance of frustrated magnetic state of the *R* atoms located in between two antiferromagnetically coupled Mn layers. When the *R* sublattice possesses strong uniaxial anisotropy, the frustration prevents long-range magnetic ordering, as it was observed for $La_{1-x}Tb_xMn_2Si_2$ at $0.2 < x \leq 0.4$ [15]. If the *R*-Mn exchange is strong enough, the origin of magnetic frustration can be eliminated by change of the interlayer Mn-Mn order from antiferromagnetic to ferromagnetic [14, 15]. For $GdMn_2Si_2$, to avoid magnetic frustration, non-collinear magnetic structure in which Gd magnetic moments lie in the basal plane is formed at $T < T_{Gd}$. Magnetic properties of the non-collinear magnetic structure of $GdMn_2Si_2$ can be described within three-sublattice model based on the Yafet-Kittel approximation.

Acknowledgments

The research was carried out within the state assignment of Minobrnauki of Russia (themes “Magnet”, “Flux” and “Alloys”) and supported in part by RFBR (project No. 18-02-00294). We acknowledge the support of the HLD-HZDR, member of the European Magnetic Field Laboratory (EMFL).

References

1. A. Szytuła and J. Leciejewicz 1989 *Handbook on the Physics and Chemistry of Rare Earths* vol 12, ed K A Gschneidner Jr and L Eyring (Amsterdam: Elsevier) p. 133.
2. A. Szytuła in K. H. J. Buschow (Ed.) *Handbook of Magnetic Materials*, vol. 6, Elsevier, Amsterdam, 1991, p. 85.
3. E. Duman, M. Acet, I. Dincer, A. Elmali, Y. Elerman. Magn. Magn. Mater. **309** (2007) 40-53.
4. B. Emre, I. Dincer, M. Hoelzel, A. Senyshyn, Y. Elerman, J. Magn. Magn. Mater. **324** (2012) 622-630.
5. Chunsheng Fang, Guoxing Li, Jianli Wang, W. D. Hutchison, Q. Y. Ren, Zhenyan Deng, Guohong Ma, Shixue Dou, S. J. Campbell, Zhenxiang Cheng. Scientific Reports **7** (2017) 45814.

6. Guoxing Li, Jianli Wang, Zhenxiang Cheng, Qingyong Ren, Chunsheng Fang, Shixue Dou. J. Appl. Phys. Lett. **106** (2015) 182405.
7. J. L. Wang, L. Caron, S.J. Campbell, S.J. Kennedy, M. Hofmann, Z.X. Cheng, M.F. Md Din, A.J. Studer, E. Bruck, S.X. Dou. Phys. Rev. Lett. **110** (2013) 217211.
8. M. F. Md Din, J.L. Wang, Z. X. Cheng, S.X. Doul, S.J. Kennedy, M. Avdeev, S.J. Campbell. Scientific Reports **5** (2015) 11288.
9. E.G. Gerasimov, M.I. Kurkin, A.V. Korolyov, V.S. Gaviko, Physica B **322** (2002) 297-305.
10. E. G. Gerasimov, N. V. Mushnikov, T. Goto. Phys. Rev. B **72** (2005) 064446.
11. E.G. Gerasimov, R.Y. Umetsu, N.V. Mushnikov, A. Fujita, T. Kanomata. J.Phys.: Condens. Matter **19** (2007) 486202.
12. T. Shigeoka, N. Iwata, H. Fujii, T. Okamoto, J. Magn. Magn. Mater. **54–57** (1986) 1343-1344.
13. M. Kolenda, J. Leciejewicz, A. Szytula, N. Sttisser, Z. Tomkowicz, J. Alloys Compd. **241** (1996) L1-L3.
14. E.G. Gerasimov, N.V. Mushnikov, P.B. Terentev, K.A. Yazovskikh, I.S. Titov, V.S. Gaviko, Rie Y. Umetsu. J. Magn. Magn. Mater. **422** (2017) 237.
15. E.G. Gerasimov, N.V. Mushnikov, P.B. Terentev, A.N. Pirogov. Journal of Alloys and Compounds **731** (2018) 397-402.
16. E.G. Gerasimov, P.B. Terentev, N.V. Mushnikov, V.S. Gaviko. Journal of Alloys and Compounds **769** (2018) 1096-1101.
17. M. Sato, Y. Ishii. Journal of Applied Physics **66** , (1989) 983.
18. Y. Skourski, M. D. Kuz'min, K. P. Skokov, A. V. Andreev, J. Wosnitza. Phys. Rev. B **83** (2011) 214420.
19. J. Rodriguez-Carvajal. Phys. B **192** (1993) 55.
20. E.G. Gerasimov, V.S. Gaviko, V.N. Neverov, A.V. Korolyov. Journal of Alloys and Compounds **343** (2001) 14.
21. A.Yu. Sokolov, Guo Guanghua, S.A. Granovski, R.Z. Levitin, H. Wada, M. Shiga, T. Goto, JETP **89** N4 (1999) 723-733.
22. N.P. Kolmakova, A.A. Sidorenko, R.Z. Levitin. Low Temperature Physics **28** (2002) 653.
23. Y. Yafet and C. Kittel. Phys. Rev. **87** (1952) 290.
24. A.F. Gubkin and H.E. Fischer. (2018). Magnetic structure of the ternary $GdMn_2Si_2$ compound and short-range magnetic order in Tb_3Ni. Institut Laue-Langevin (ILL) doi:10.5291/ILL-DATA.EASY-290.
25. H.E. Fischer, G.J. Cuello, P. Palleau, D. Feltin, A.C. Barnes, Y.S. Badyal and J.M. Simonson. Applied Physics A **74** (2002) S160-S162.

26. S.A. Granovsky, A. Kreyssig, M. Doerr, C. Ritter, E. Dudzik, R. Feyerherm, P.C. Canfield, M. Loewenhaupt. J. Phys.: Condens. Matter **22** (2010) 226005.
27. G. Venturini, R. Welter, E. Ressouche, B. Malaman, J. Magn. Magn. Mater. **150** (1995) 197-212.
28. Welter R., Venturini G., Fruchart D., Malaman B. Journal of Alloys and Compounds **191** (1993) 263–270.
29. G. Venturini, R. Welter, E. Ressouche, B. Malaman Journal of Alloys and Compounds **223** (1995) 101.
30. K.P. Belov, A.K. Zvezdin, A.M. Kadomtseva, R.Z. Levitin, Sov. Phys. Uspekhi **19** (1976) 574.
31. A.S. Ermolenko, IEEE Trans. Magn. **MAG-15** (1979) 1765.
32. M.D. Kuzmin, Phys. Rev. B **46** (1992) 8219.

- Magnetic structures have been determinated for the $GdMn_2Si_2$ compound with layered crystal structure at temperatures 10 and 300 K.
- $GdMn_2Si_2$ has strong easy plane type magnetic anisotropy at temperatures $T_{Gd} < 52$ K at which Gd atoms are magnetically ordered.
- The Mn sublattice has uniaxial anisotropy with the easy *c* axis.
- Easy plane magnetic anisotropy of $GdMn_2Si_2$ arises to prevent magnetic frustration in Gd layers.
- Magnetic properties of $GdMn_2Si_2$ at $T < 52$ K can be described within a three-sublattice model based on the Yafet-Kittel approximation.

Declaration of interests

☒ The authors declare that they have no known competing financial interests or personal relationships that could have appeared to influence the work reported in this paper.